



Atomic simulation for influence of helium atom on movement of edge dislocation in nickel

Xi-yuan YANG

Physics Science and Technology School, Lingnan Normal University, Zhanjiang 524048, China

Received 21 November 2014; accepted 20 March 2015

Abstract: The molecular dynamics (MD) simulation and the modified analytical embedded-atom method (MAEAM) were used to study the influence of a He atom on the movement of the $(a/2)\langle 110 \rangle \{1\bar{1}1\}$ edge dislocation in Ni. First, the calculated Burgers vector distribution shows that the equilibrium dissociation distance (D_{ed}) and the stacking fault energy (E_{sf}) between two partial edge dislocations are about 25.95 Å and 108 mJ/m², respectively. Then, the obtained formation energies (E_f) of a He atom at some different sites demonstrate that the He atom is attracted and repelled in the tension and compression regions, respectively. And the He–dislocation interaction reveals that an interstitial He atom plays a more significant role in the dislocation movement than a substitutional He atom. Finally, it is found that the movement of an interstitial He atom is apparent as the first partial dislocation bypasses and the edge dislocation offers fast-diffusion path for the migration of a He atom.

Key words: movement; edge dislocation; He; atomic simulation; Ni

1 Introduction

It is known that the crystalline material generally contains abundant dislocations, which are dramatically responsible for the variation in the mechanical properties [1,2]. In particular, the movement of the dislocation and its interaction with other defects are important to understand the irradiation damage and mechanical properties. The degradation in the mechanical strength with a long-term exposure to irradiation has been enslaved to produce abundant defects, which could form some effective blocking barriers to hinder the dislocation movement under the external stress [3–5]. And the plastic deformation of materials results mainly from the movement of the dislocation in the crystal [6]. Hence, it is interesting to study the movement of the dislocation and its interaction with other defects [7–11].

With the development of the computational technique, molecular dynamics (MD) simulation has been proved to be a useful tool to study the impeditive influence of defect obstacles on the movement of the dislocation [12,13]. MORISHITA et al [14,15] used MD to study the migration energy and the binding energy of a He atom and its interaction with other defects in α -Fe,

which demonstrated that the He atom was strongly trapped in a single vacancy. HEINISCH et al [16] studied the formation energy and the binding energy of the interstitial He atom in or near a dislocation core. The obtained results indicated that the interstitial He atom had a negative binding energy in the compression region and a strongly positive binding energy in the tension region. NEDELCOU et al [17] found that a H atom in the Fe matrix could block the dislocation movement, and the stress exerted on the dislocation could reach 15.5 MPa. The interstitial H atom strongly impeded the movement of the dislocation and gave a maximal value of stress (~38.2 MPa) before the dislocation passing by. OSETSKY et al [18–20] constructed an atomic-level model to interpret the dislocation movement and the inherent mechanisms of the dislocation–obstacle interaction.

In fact, at low temperatures, He atoms also induced the irradiation hardening phenomenon [21] and the degradation of material lifetime [22], which could be deduced from the reaction between He and dislocation. He atom assembled to form a cluster and impeded the dislocation movement [23]. Moreover, the irradiation hardening phenomenon of structural materials in the nuclear reaction was primarily affected by the

interactions between dislocation and other obstacles [24,25]. The effect of the He atom on the decrease of fracture toughness of the reduced-activation steels was so crucial that the He atom further resulted in a significant change in the mechanical properties of nuclear materials. In addition, since its solubility in metallic material was extremely low, He tended to precipitate into clusters or bubbles and produced void swelling and surface roughing. Ni, as a corrosion-resistant material with very good formability, was usually used to improve the mechanical properties of Fe material [26,27].

2 Methodology

A simulation system, where about 20000 Ni atoms are assigned in a simulation box, is first constructed. The sizes of the simulation box are about $21a \times 17a \times 17a$ in the x , y and z directions, respectively. The alphabet $a=0.3156$ nm represents the lattice parameter of the crystalline Ni. The coordinate axes x , y and z of the simulation box are oriented in $[110]$, $[1\bar{1}1]$ and $[\bar{1}12]$ directions, respectively. The real length of the box is about 7.5, 6 and 6 nm, respectively. The method of obtaining the edge dislocation was described in detail in Ref. [28]. The stable configuration with two straight edge partial dislocations along the $\langle\bar{1}12\rangle$ direction is shown in Fig. 1. Periodic boundary conditions are applied in the x -axis and z -axis directions, whereas fixed boundary condition is employed in the y -axis direction. The atoms in the region of upper and lower three $(1\bar{1}1)$ crystalline planes are rigidly fixed, whereas other atoms can move freely. The glide force acting on the dislocation is generated by the relative displacement of the rigid blocks in the x direction.

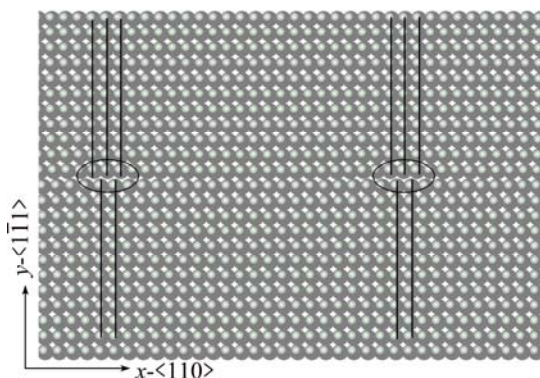


Fig. 1 Planar structure of $(a/2)\langle 110 \rangle \{1\bar{1}1\}$ edge dislocation perpendicular to $\langle\bar{1}12\rangle$ direction (Black lines denoted sites of partial dislocations)

Two potential functions are introduced to depict the atomic interactions. The modified analytical embedded-atom method (MAEAM) potential, which has been successfully used to study the physical properties of

metallic materials [29,30], is adopted to describe the metallic atom interactions. And the interactions between He and Ni atoms are treated by the Morse potential [31]. These empirical potentials and the corresponding technical details were explicitly reported elsewhere [29].

3 Results and discussion

3.1 Distribution of burgers vector

After the simulation system is adequately relaxed at 0 K, the rearranged atoms in double $(1\bar{1}1)$ planes adjacent to the slip plane are plotted in Fig. 2, where two partial dislocations are clearly confirmed by the different stacking segments as surrounded by rectangles. Here, the position of each partial dislocation could be accurately identified by the distribution of the Burgers vector [32], which is defined as the disregistry of the misfit displacement between neighbor atoms in both adjacent $(1\bar{1}1)$ glide planes with respect to the x coordinate, as shown in Fig. 3. The maximal disregistry

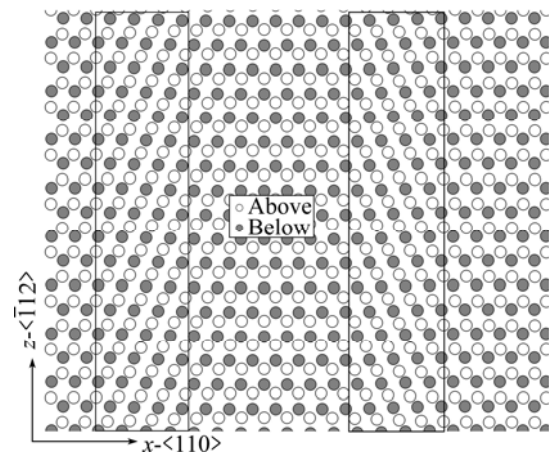


Fig. 2 Equilibrium crystalline sites of atoms in two adjacent $(1\bar{1}1)$ planes below (open circles) and above (solid circles) slip plane

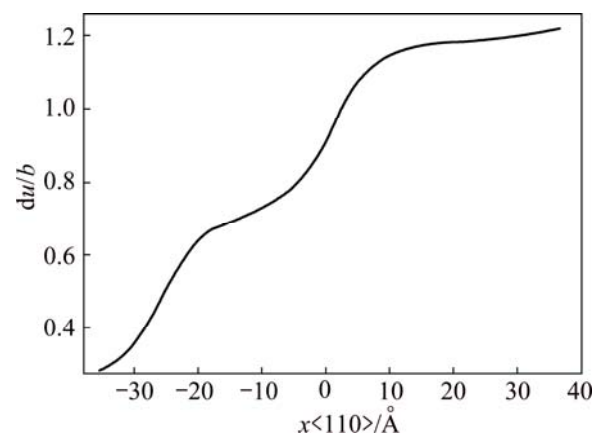


Fig. 3 Disregistry of differential displacement between atoms in two neighbor atomic planes adjacent to slip plane in $\langle 110 \rangle$ direction

of the misfit displacement represents the position of the partial dislocation. The plotting profiles of the Burgers vector distribution are clearly plotted in Fig. 4. The position of each partial dislocation is associated with the maximum of distribution as similar to the description in Fig. 3. The equilibrium dislocation distance (D_{ed}) of the double partial dislocations is estimated from Fig. 4. Correspondingly, the stacking fault energy (E_{sf}) is calculated according to $E_{sf}=(Gb_1 \cdot b_2)/(2\pi d)$ described in Ref. [33], where G is the shear modulus, b_1 and b_2 are the Burgers vectors of the partial dislocation, respectively. The calculated values of D_{ed} and E_{sf} are summarized in Table 1, where it can be found that these calculated results are in reasonable agreement with the previously theoretical and experimental results.

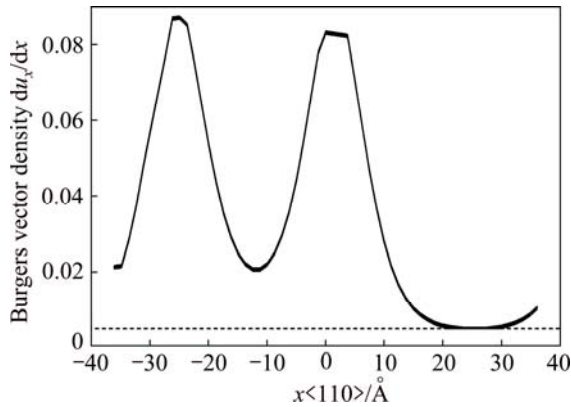


Fig. 4 Distribution of Burgers vector as function of x coordinate

Table 1 Calculated and referenced values of D_{ed} and E_{sf} for Ni

Reference	$D_{ed}/\text{Å}$	$E_{sf}/(\text{mJ}\cdot\text{m}^{-2})$
EXP [35]	26±8	120–130
EAM [36]	30, 21	–
EAM [37]	25	–
TB [38]	–	305 (0 K), 262 (300 K)
EAT [39]	28–32	100
This work	25.95	108

3.2 Formation energy of He atom

To study the He–dislocation interaction, the formation energy (E_f) is calculated with the following formula [29]:

$$E_f(\text{He}) = E_{\text{tot}}(\text{disloc} + \text{He}) - \{\varepsilon_{\text{He}} + E_{\text{tot}}(\text{disloc})\} \quad (1)$$

where $\varepsilon_{\text{He}} = -0.0071$ eV is the cohesive energy of a He atom in the perfect crystal [14,15], $E_{\text{tot}}(\text{disloc} + \text{He})$ and $E_{\text{tot}}(\text{disloc})$ represent the total energies of the simulation system with and without a He atom, respectively. The total energies are obtained after the simulation system was fully relaxed at 0 K. According to Eq. (1), the E_f of a He atom is calculated at the different sites along a straight line by passing one of the partial

dislocations from the compression region to the tension region. The formation energies of the interstitial and substitutional He atom at each crystalline site are shown in Figs. 5 (a) and (b), respectively.

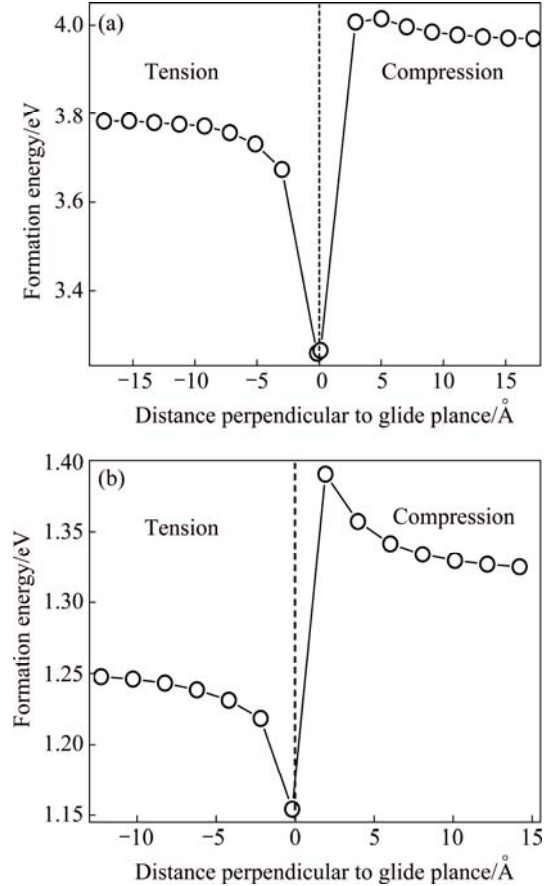


Fig. 5 E_f of He atom as function of their distance along straight line through partial dislocation core normal to glide plane in tension and compression regions: (a) Interstitial He atom; (b) Substitutional He atom

From Fig. 5, it can be seen that the variation tendency of E_f is generally similar for the behaviors of interstitial and substitutional He atoms. But the E_f values of interstitial atom are significantly larger than those of substitutional atom, which indicates that the influence of interstitial He atom on the movement of dislocations is stronger. At the core region, the minimal values of E_f for the interstitial and substitutional He atoms are about 3.26 eV and 1.15 eV, respectively, which are significantly lower than those at other crystalline sites. These cases imply that the He atom is easily trapped by the dislocation regardless of the interstitial or substitutional sites, and correspondingly hinders the movement of dislocation, which is similar to the role of the He atom in the grain boundary [34]. In addition, the E_f of He atom locating at the interstitial and substitutional sites in the tension region reduces with decreasing the He–dislocation separation distance. And

relative to the maximum of E_f in the glide region, the decreasing amplitude of E_f of the interstitial He atom is about 0.52 eV, which is distinctly greater than that of the substitutional He atom (~ 0.093 eV). It illustrates that there is a driven force to induce the He atom moving into the glide field in the tension region and divorcing from the glide field in the compression region. From Figs. 5(a) and (b), it can further find out that the position dependence of the E_f value of He atom is significantly different in the tension and compression regions. The E_f value gradually increases with decreasing the He–dislocation distance in the compression region. It demonstrates that the He atom needs to overcome the resistive energy barrier to migrate into the dislocation core region from the compression region. The resistive energy barrier leads to a decline of He atom dependence of the dislocation. The resistive energy barrier, which is obtained from the difference between the maximum and minimum values of E_f , is about 0.037 eV for the interstitial He atom and 0.065 eV for the substitutional He atom in the compression region. Clearly, for the substitutional He atom, the resistive barrier resulted from the matrix in the compression region is strong, which means that the substitutional He atom migrates difficultly to the core and makes little impact on the dislocation movement. On the contrary, in the tension region, the E_f value decreases as the He–dislocation distance decreases, which indicates that the He atom assembles easily into the dislocation core region and forms clusters to impede the dislocation movement. Relatively, the change of E_f value of the interstitial He atom is large. The dislocation movement is mainly controlled by the interstitial He atom. The similar results were also described in the previous studies of HEINISCH et al [16].

3.3 Influence of He atom on movement of dislocation without external applied strain

To understand the He–dislocation interaction, the binding energy of the He–dislocation is further discussed, of which the calculated method was described in Ref. [11]. Firstly, the interstitial and substitutional He atoms are inserted into the central site between the partial dislocations. After the system is fully relaxed without external strain, the binding energies of the interstitial and substitutional He atoms are about 0.51 and 0.13 eV, respectively. The calculated values of binding energy demonstrate that the interaction of the interstitial He atom and the dislocation is more significant than that of the substitutional He atom and the dislocation, which is similar to the conclusions obtained by discussing the formation energy mentioned above. These cases further indicate that the interstitial He atom plays a leading role in the movement of dislocation and the effect of substitutional He atom is basically ignored.

Certainly, the interaction between the interstitial He atom and the dislocation can be further verified by the atomic snapshots of edge dislocation. In terms of the common neighbor analysis [40], it can distinguish the atoms in the dislocation region from all of Ni atoms. The visualized atomic snapshots of dislocation movement including the substitutional and interstitial He atoms are shown in Figs. 6 and 7, respectively. From Fig. 6, it can be seen that the shape of the dislocation line always keeps straight and the distance between the He atom and

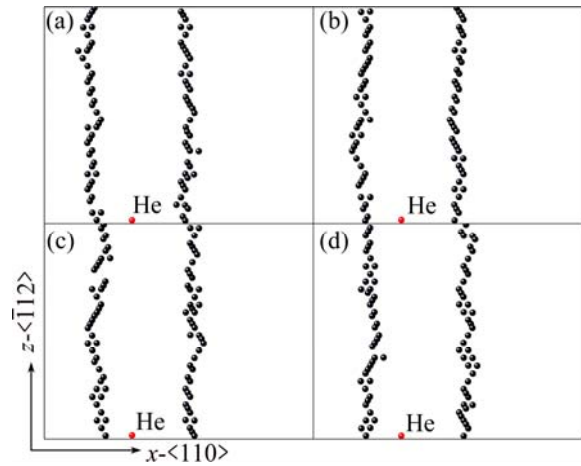


Fig. 6 Atomic snapshots for relaxed time dependence of dislocation and substitutional He atom: (a) 7 ps; (b) 8 ps; (c) 9 ps; (d) 10 ps (Only dislocation core atoms and He atom are shown, and red and black circles represent He and Ni atoms, respectively)

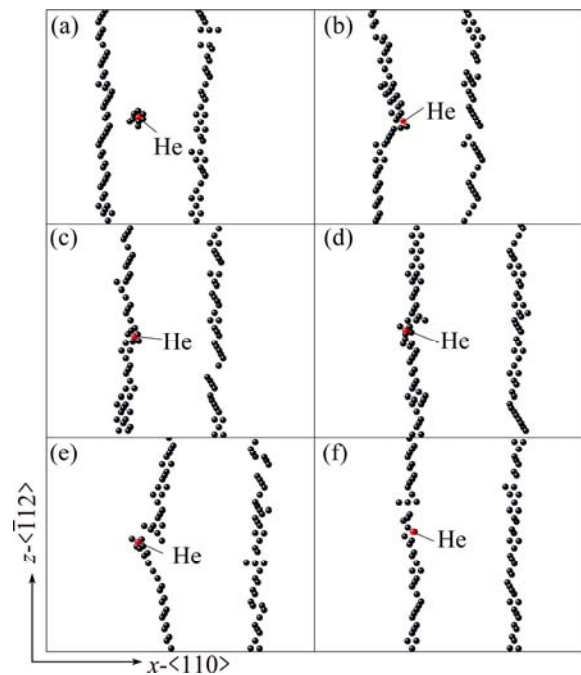


Fig. 7 Atomic snapshots of specimen including dislocation and interstitial He atom with different relaxed time: (a) 7 ps; (b) 8 ps; (c) 9 ps; (d) 11 ps; (e) 13 ps; (f) 15 ps (Only core atoms and He atom are shown, and red and black circles represent He and Ni atoms, respectively)

the dislocation changes little, which indicates that the interaction between the substitutional He atom and the dislocation is so weak that it can be negligible. Hence, it focuses on the influence of the interstitial He atom on the dislocation movement.

Figure 7 shows that the interaction between the interstitial He atom and the partial dislocation is more apparent. The interstitial He atom is first replaced in the middle of both partial dislocations. Because of the He–dislocation interaction, the dislocation gradually bends toward the interstitial He atom and gradually moves to it, as described in Figs. 7(a) and (b). Apparently, the cusp angle of the bending dislocation means that the He atom offers an attractive influence on the edge dislocation. Furthermore, after the prior partial dislocation arrives, the interstitial He atom moves incessantly in the glide plane for its inherent inertia, which is shown in Figs. 7(c) and (d). Then in Fig. 7(e), a reversely sharp cusp angle indicates that the dislocation is pinned by the interstitial He atom. Because the velocity of the dislocation is not strong enough to overcome the pinning effect of the interstitial He atom, the flexural dislocation gradually gets back to the original shape as a result of the action of its internal tension and the interstitial He atom trapped by the prior partial dislocation. The similar results were also obtained by DOYAMA et al [41]. On the basis of these facts discussed above, the interstitial He atom obviously offers a stronger effect on the dislocation movement in comparison with the substitutional He atom. The reasons for the behaviors may be as follows: the interstitial He atom heavily deforms the surrounding crystalline configuration for the asymmetric interaction with the matrix Ni atom. Correspondingly, the formation energy of the interstitial He atom is drastically elevated to strengthen its interaction with the dislocation, as described in Fig. 7. On the contrary, for the symmetrical force deriving from the matrix atoms, the substitutional He atom makes the shape of crystalline structure change little which leads to the slight interaction with the dislocation, as described in Fig. 6.

3.4 Influence of interstitial He atom on dislocation movement with external applied strain

On the basis of the above discussion, this work aims at the effect of the interstitial He atom on the dislocation movement under external applied strain. The He atom is originally placed in a dislocation core region. Then, for every 20000 time steps, a shear strain ($\sim 0.02\%$) is imposed to the atoms of the upper three fixed layers which are perpendicular to the $y[1\bar{1}1]$ direction. The whole process of the dislocation movement is shown in Fig. 8. Under the external strain, the trailing partial dislocation is impeded by the interstitial He atom, as

described in Figs. 8(a) and (b). But at the same time, the approaching dislocation can offer space for the movement of interstitial He atom. Thus, the interstitial He atom is easily trapped by the provisionally produced vacancies, and results in the attractive action on the dislocation, which is in agreement with the previous investigations [12,13]. Because of the inertia of the moving dislocation and the external strain, the dislocation successfully overcomes the pinning effect of the interstitial He atom and moves forward continuously. In Figs. 8(b) and (c), the depinning effect of the He atom occurs. As the dislocation bypasses over the interstitial He atom, a backward cusp angle can be recognized, which indicates that there is an obstructed force before the dislocation leaves from the He atom. After deviating from the pulling effect of the interstitial He atom, the line dislocation can move continually without resistance, as described in Fig. 8(d).

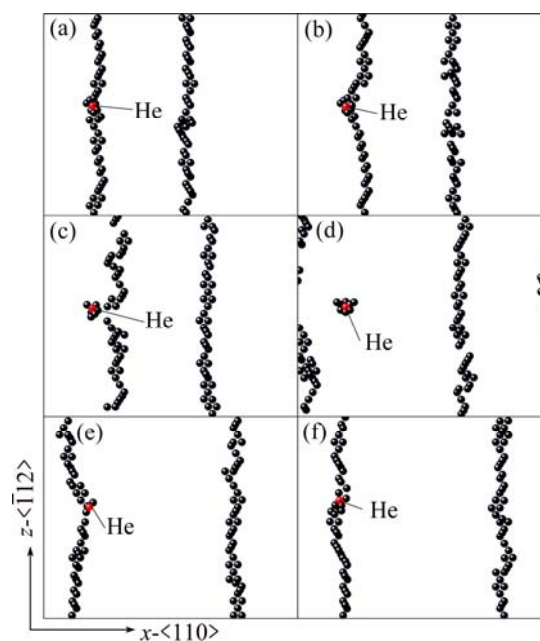


Fig. 8 Atomic snapshots of dislocation movement with He atom under applied shear strains with different relaxed time: (a) 6.75 ps; (b) 7.25 ps; (c) 7.75 ps; (d) 13.75 ps; (e) 15.5 ps; (f) 16.25 ps (Only core atoms and He atom are shown, and red and black circles represent He and Ni atoms, respectively)

As a result of the periodic boundary condition, the leading partial dislocation passes over the boundary to gradually approach the interstitial He atom again. And the shape of this partial dislocation gradually bends out toward the interstitial He atom as a result of the attraction effect, as shown in Fig. 8(e). Finally, with the tensile force and the inertia of the dislocation movement, the dislocation becomes straight again, such as the description of Fig. 8(f), and then repeats the forgoing evolution. In the simulated process, the interstitial He

atom, as an obstacle, obviously gives a pinning impact on the dislocation movement, which is similar to those of the previous studies [42,43].

3.5 Movement of interstitial He atom under applied strain

In general, an interstitial He atom is apt to locate at the stable octahedral site of the perfect FCC crystal. However, as the dislocation crosses over, the crystalline configuration is deformed, which leads to the decline of energy barrier of the impure atoms. Thus, the interstitial atom can easily overcome the energy barrier to leave the original site to the other stable one [16]. Figure 9 shows the migration course of the He atom. The solid circles represent the matrix Ni atoms. The alphabets α , β and γ , which are denoted with the dash circles, represent three different stable crystalline sites of the He atom because of the He atom movement. The stable α site denotes the original one before the partial dislocation gets across. And the stable β and γ sites denote the new equilibrium ones as a partial dislocation bypasses, respectively. That is to say, the $\alpha \rightarrow \beta$ process implies that the first partial dislocation crosses over the He atom. The $\beta \rightarrow \gamma$ process, which denotes the He atom migrates from the stable β site to stable γ site, indicating that the second partial dislocation gets through the He atom. In Fig. 9, it is shown that the migration distance of the He atom in the first process is much larger than that of the second process. Compared with the second partial edge dislocation, the first partial edge dislocation apparently impacts much more on the movement of interstitial He atom. The reason will be analyzed in the following.

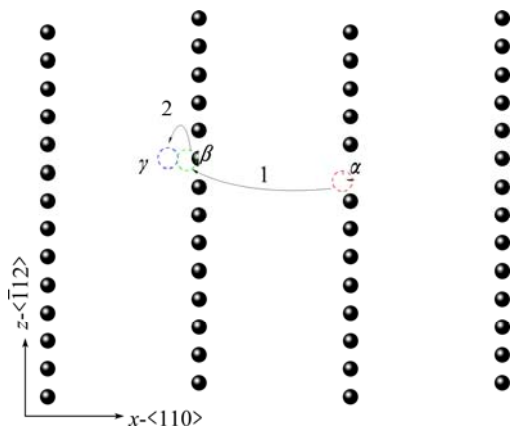


Fig. 9 Rearrangement of interstitial He atom in edge dislocation region

To investigate the migration process of the interstitial He atom, the relaxation time dependence of the separation distances Δr between an instantaneous site of the He atom and its corresponding three stable ones, as shown in Fig. 9, is calculated. The calculated method is expressed as follows:

$$\Delta r = \sqrt{(x - x_i)^2 + (y - y_i)^2 + (z - z_i)^2}, (i = \alpha, \beta, \gamma) \quad (2)$$

The separation distances Δr , defined as the difference between an instantaneous site of the He atom and its three equilibrium sites, are solved by $\Delta x = x - x_i$, $\Delta y = y - y_i$, $\Delta z = z - z_i$ ($i = \alpha, \beta, \gamma$) in the x , y and z directions, respectively. The time dependence of the separation distances is plotted in Fig. 10, where the processes of the partial dislocations bypassing the He atom are demarcated with the shaded region in each graph.

The investigations mentioned above reveal the dislocation dependence of the general movement of the interstitial He atom. In fact, the migration processes of the He atom in all directions are apparently different. In order to display the influence of the dislocation on the migration of the He atom, the variation tendencies in the migration distances Δx , Δy and Δz in the x , y and z directions in the simulation process are first studied, which are plotted in Figs. 10(a), (b) and (c), respectively. In comparison with the magnitude of Δx , Δy and Δz at the initial and last stages, it can be found out that the migration distance in the Δz direction (i.e., the dislocation line direction) (Fig. 10(c)) is about 4 Å, which is apparently larger than that in other directions. The results indicate that the partial dislocation provides the preferential fast-diffusion path for the migration of the He atom. In Fig. 10(b), the migration distance Δy is less than zero, which demonstrates that the interstitial He atom moves to the tensile region. There are two obvious concave regions for each curve, which mean that the partial dislocations pass through the He atom. According to the studies of EDMONDSON et al [44], the He atom assembled easily to form He bubbles with thermal stability in these regions. In addition, from Fig. 10(b), it can be seen that the sinking depth Δh_1 (≈ 0.8 Å) of the first concave is smaller than Δh_2 (≈ 2.5 Å) of the second one. The larger depth magnitude of the He atom indicates that the interstitial He atom impregnates more deeply into the tension region and is far away from the glide plane at the period of the dislocation passing over. Thereby, the bypassing dislocation gives rise to relatively slight effects on the migration of the He atom. The case can be also shown as the description of the red and green curves in Figs. 10(a) and (c) as well as the green and blue circles in Fig. 9. In Fig. 10(a), the fluctuation characteristics of three curves are very similar. It demonstrates that the He atom migrates little in the $\beta \rightarrow \gamma$ process along the x direction for the similar reasons mentioned above.

However, in Fig. 10(d), the black, red dashed and green dot-dashed curves denote the time dependence of the total migration distances between the instantaneous site of the He atom and its three stable α , β , and γ sites, respectively. It is clearly demonstrated that, with

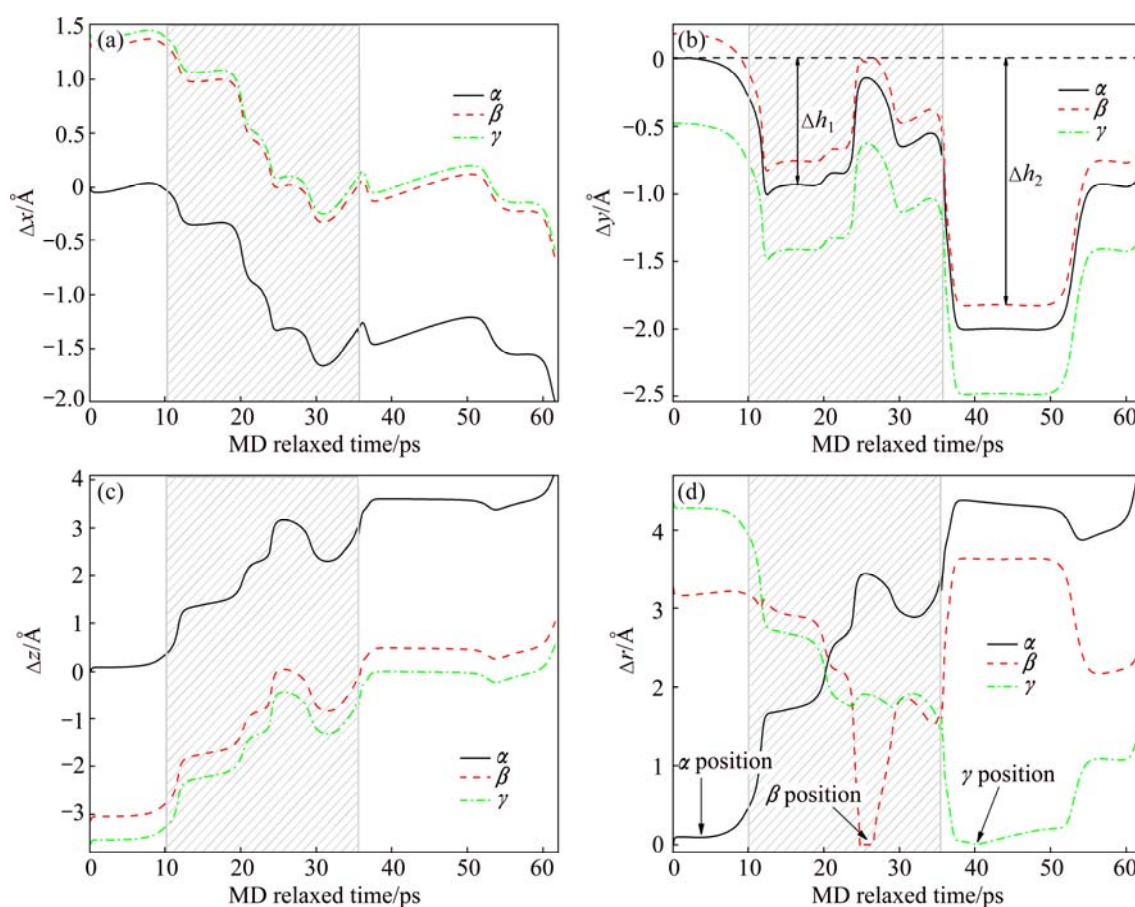


Fig. 10 Variations in distances between instantaneous site of He atom and its three stable sites α , β and γ as similarly denoted in Fig. 9: time dependence of distance Δx (a), Δy (b), Δz (c) and Δr (d) (Shaded region represents partial dislocation gets through interstitial He atom)

approximating rapidly to the He atom, the first partial dislocation decreases the migration energy barrier and induces the He atom to break away from its original α site, which indicates that the partial dislocation attracts the He atom similar to the description of Figs. 7(b) and 8(e). The concrete features are that the separation distance between the He atom and the α site increases quickly, as described by the black curve in Fig. 10(d). Accordingly, the migration distance between the instantaneous site of the He atom and its stable β site rapidly decreases with the relaxed time ranging from 10 to 25 ps, as shown by the red dashed curve in Fig. 10(d). When the first partial dislocation crosses over, the interstitial He atom glides rapidly into the β site in the stacking fault ribbon region and the separation distance between the instantaneous and stable β sites of the He atom reduces to nearly zero. It exhibits that the interstitial He atom can get into the stable β site. Thus, the $\alpha \rightarrow \beta$ migration process of the He atom is finished. Then, the second partial dislocation is gradually close to the He atom, the distance of which separating to the stable β site increases swiftly. The second partial dislocation first impels the He atom to deviate from the

stable β site, which results in the distance increasing significantly from 25 to 30 ps. When the second partial dislocation passes through, the migration distance between the instantaneous and stable γ sites of the He atom decreases apparently, as described by the green dash-dotted curve in Fig. 10(d). It indicates that the $\beta \rightarrow \gamma$ migration process of the He atom is completed. In addition, at each time of the dislocation leaving from the He atom, there is a significantly depinning interaction between the He atom and the edge dislocation.

4 Conclusions

1) The distribution of the Burgers vector shows that the dislocation in the glide plane splits into two partial dislocations. The calculated D_{ed} and E_{sf} are about 25.95 Å and 108 mJ/m², respectively.

2) The obtained formation energy of the He atom indicates that there is driven force in the tension region and resisted force in the compression region. The depinning effect of the interstitial He atom on the dislocation movement is more significant than that of the substitutional He atom.

3) The separation distances between the He atom and its three stable sites are investigated. The results indicate that the interstitial He atom migrates more apparently as the first partial dislocation slips and the dislocation provides pipe fast-diffusion path for the migration of the He atom.

References

- [1] RODNEY D. Molecular dynamics simulation of screw dislocations interacting with interstitial frank loops in a model FCC crystal [J]. *Acta Materialia*, 2004, 52(3): 607–614.
- [2] SOLEYMANI M, PARSA M H, MIRZADEH H. Molecular dynamics simulation of stress field around edge dislocations in aluminum [J]. *Computational Materials Science*, 2014, 84(3): 83–96.
- [3] HATANO T, MATSUI H. Molecular dynamics investigation of dislocation pinning by a nanovoid in copper [J]. *Physical Review B*, 2005, 72(9): 094105.
- [4] MU J W, SUN S C, JIANG Z H, LIAN J S, JIANG Q. Dislocation-mediated creep process in nanocrystalline Cu [J]. *Chinese Physics B*, 2013, 22(3): 037303.
- [5] TAPASA K, OSETSKY Y, BACON D J. Computer simulation of interaction of an edge dislocation with a carbon interstitial in α -iron and effects on glide [J]. *Acta Materialia*. 2007, 55(1): 93–104.
- [6] XU S, GUO Y F, NGAN A H W. A molecular dynamics study on the orientation, size, and dislocation confinement effects on the plastic deformation of Al nanopillars [J]. *International Journal of Plasticity*, 2013, 43(4): 116–127.
- [7] SHIN I, CARTER E A. Simulations of dislocation mobility in magnesium from first principles [J]. *International Journal of Plasticity*, 2014, 60(9): 58–70.
- [8] XU Q, YAMASAKI H, SUGIURA Y, SATO K, YOSHIIE T. Effects of interactions between dislocations and/or vacancies and He atoms on mechanical property changes in Ni [J]. *Materials Science and Engineering A*, 2013, 586(12): 231–235.
- [9] SONG H, WANG Z J. Effect of electropulsing on dislocation mobility of titanium sheet [J]. *Transactions of Nonferrous Metals Society of China*, 2012, 22(7): 1599–1605.
- [10] TEREITYEV D, ANENTO N, SERRA A, ORTIZ C J, ZHURKIN E E. Interaction of He and He–V clusters with self-interstitials and dislocations defects in bcc Fe [J]. *Journal of Nuclear Materials*, 2015, 458(1): 11–21.
- [11] CLOUET E, GARRUCHET S, NGUYEN H, PEREZ M, BECQUART C S. Dislocation interaction with C in α -Fe: A comparison between atomic simulations and elasticity theory [J]. *Acta Materialia*, 2008, 56(14): 3450–3460.
- [12] YANG L, ZHU Z Q, PENG S M, LONG X G, ZHOU X S, ZU X T, HEINISCH H L, KURTZ R J, GAO F. Effects of temperature on the interactions of helium–vacancy clusters with gliding edge dislocations in α -Fe [J]. *Journal of Nuclear Materials*, 2013, 441(1–3): 6–14.
- [13] XU Q, YAMASAKI H, SUGIURA Y, SATO K, YOSHIIE T. Effects of interactions between dislocations and/or vacancies and He atoms on mechanical property changes in Ni [J]. *Materials Science and Engineering A*, 2013, 586(12): 231–235.
- [14] MORISHITA K, SUGANO R, WIRTH B D. MD and KMC modeling of the growth and shrinkage mechanisms of helium–vacancy clusters in Fe [J]. *Journal of Nuclear Materials*, 2003, 323(2–3): 243–250.
- [15] MORISHITA K, SUGANO R, WIRTH B D, DIAZ DE LA RUBIA T. Thermal stability of helium–vacancy clusters in iron [J]. *Nuclear Instruments and Methods in Physics Research Section B*, 2003, 202(4): 76–81.
- [16] HEINISCH H L, GAO F, KURTZ R J, LE E A. Interaction of helium atoms with edge dislocations in α -Fe [J]. *Journal of Nuclear Materials*, 2006, 351(1–3): 141–148.
- [17] NEDELCO S, KIZLER P. Molecular dynamics simulation of hydrogen–edge dislocation interaction in BCC iron [J]. *Physica Status Solidi (a)*, 2002, 193(1): 26–34.
- [18] OSETSKY YU N, BACON D J. An atomic-level model for studying the dynamics of edge dislocations in metals [J]. *Modelling and Simulation in Materials Science and Engineering*, 2003, 11(4): 427–446.
- [19] OSETSKY YU N, BACON D J, MOHLES A V. Atomic modeling of strengthening mechanisms due to voids and copper precipitates in α -iron [J]. *Philosophical Magazine*, 2003, 83(31–34): 3623–3641.
- [20] OSETSKY YU N, BACON D J. Void and precipitate strengthening in α -iron: What can we learn from atomic-level modelling [J]. *Journal of Nuclear Materials*, 2003, 323(2–3): 268–280.
- [21] LUO F F, YAO Z, GUO L P, SUO J P, WEN Y M. Convolved dislocation loops induced by helium irradiation in reduced-activation martensitic steel and their impact on mechanical properties [J]. *Materials Science and Engineering A*, 2014, 607(6): 390–396.
- [22] ENRIQUE M, DANIEL S, ALFREDO C. Helium segregation to screw and edge dislocations in α -iron and their yield strength [J]. *Acta Materialia*, 2015, 84(2): 208–214.
- [23] HASHIMOTO N, SAKUAYA S, TANIMOTO J, OHNUKI S. Effect of impurities on vacancy migration energy in Fe-based alloys [J]. *Journal of Nuclear Materials*, 2014, 445(1–3): 224–226.
- [24] SCHÄUBLIN R, CHIU Y L. Effect of helium on irradiation-induced hardening of iron: A simulation point of view [J]. *Journal of Nuclear Materials*, 2007, 362(2–3): 152–160.
- [25] WANG Y X, XU Q, YOSHIIE T, PAN Z Y. Effects of edge dislocations on interstitial helium and helium cluster behavior in α -Fe [J]. *Journal of Nuclear Materials*, 2008, 376(2): 133–138.
- [26] SHIM J H, KWON S C, KIM W W, WIRTH B D. Atomistic modeling of the interaction between self-interstitial dislocation loops and He in bcc Fe [J]. *Journal of Nuclear Materials*, 2007, 367–370(8): 292–297.
- [27] MARTIENSSEN W, WARLIMONT H. *Handbook of condensed matter and materials data* [M]. Springer: Berlin Heidelberg, 2005: 279–281.
- [28] HU S Y, SCHMAUDER S, CHEN L Q. Effects of dislocation-trapped helium on mechanical properties of Fe [J]. *Materials Science and Engineering A*, 2014, 612(8): 41–45.
- [29] XIA J X, HU W Y, YANG J Y, AO B Y, WANG X L. A comparative study of helium atom diffusion via an interstitial mechanism in nickel and palladium [J]. *Physica Status Solidi (b)*, 2006, 243(3): 579–583.
- [30] XIA J X, HU W Y, YANG J Y, AO B Y, WANG X L. A study of the behavior of helium atoms at Ni grain boundaries [J]. *Physica Status Solidi (b)*, 2006, 243(12): 2702–2710.
- [31] BASKES M I, MELIUS C F. Pair potentials for FCC metals [J]. *Physical Review B*, 1979, 20(8): 3197–3204.
- [32] HÄKKINEN H, MÄKINEN S, MANNINEN M. Edge dislocations in fcc metals: Microscopic calculations of core structure and positron states in Al and Cu [J]. *Physical Review B*, 1990, 41(18): 12441–12453.
- [33] PAN Jin-sheng, TONG Jian-min, TIAN Min-bo. *Fundamentals of materials science* [M]. Beijing: Tsinghua University Press, 2011: 280–283. (in Chinese)
- [34] ZHOU H B, JIN S, ZHANG Y, SHU X L, NIU L L. Role of helium in the sliding and mechanical properties of a vanadium grain boundary: A first-principles study [J]. *Chinese Physics B*, 2014, 23(5): 056104.
- [35] CARTER C B, HOLMES S M. The stacking-fault energy of nickel [J]. *Philosophical Magazine*, 1977, 35(5): 1161–1172.

- [36] BITZEK E, GUMBSCH P. Dynamic aspects of dislocation motion: Atomistic simulations [J]. *Materials Science and Engineering A*, 2005, 400–401(7): 40–44.
- [37] CLOUET E. The vacancy–edge dislocation interaction in fcc metals: A comparison between atomic simulations and elasticity theory [J]. *Acta Materialia*, 2006, 54(13): 3543–3552.
- [38] MEYER R, LEWIS L J. Stacking-fault energies for Ag, Cu, and Ni from empirical tight-binding potentials [J]. *Physical Review B*, 2002, 66(5): 052106.
- [39] SATO K, YOSHIIE T, ISHIZAKI T, XU Q. Behavior of vacancies near edge dislocations in Ni and α -Fe: Positron annihilation experiments and rate theory calculations [J]. *Physical Review B*, 2007, 75(9): 094109.
- [40] HONEYCUTT J D, ANDERSEN H C. Molecular dynamics study of melting and freezing of small Lennard-Jones clusters [J]. *Journal of Physical Chemistry*, 1987, 91(19): 4950–4963.
- [41] DOYAMA M, KOGURE Y, NOZAKI T. Interactions between point defects and edge dislocations in copper [J]. *Nuclear Instruments and Methods in Physics Research Section B*, 2007, 255(1): 85–91.
- [42] DUNN A Y, MCPHIE M G, CAPOLUNGO L, MARTINEZ E, CHERKAOUI M. A rate theory study of helium bubble formation and retention in Cu–Nb nanocomposites [J]. *Journal of Nuclear Materials*, 2013, 435(1–3): 141–152.
- [43] HE Yan-sheng, FU Shi-hua, ZHANG Qing-chuan. Simulations of the interactions between dislocations and solute atoms in different loading conditions [J]. *Acta Physica Sinica*, 2014, 63(22): 228102. (in Chinese)
- [44] EDMONDSON P D, PARISH C M, LI Q, MILLER M K. Thermal stability of nanoscale helium bubbles in a 14YWT nanostructured ferritic alloy [J]. *Journal of Nuclear Materials*, 2013, 445(1–3): 84–90.

氦原子对镍金属中刃型位错运动行为影响的原子模拟

阳喜元

岭南师范学院 物理科学与技术学院, 湛江 524048

摘要: 应用分子动力学(MD)技术和改进分析型嵌入原子法(MAEAM)研究氦原子对镍金属中 $(a/2)\langle 110 \rangle\{1\bar{1}1\}$ 刃型位错迁移行为的影响。首先通过计算晶格的 Burgers 矢量分布, 确定两刃型分位错之间的平衡距离(D_{ed})约为 25.95 Å, 而它们之间的堆垛层错能(E_{sf})约为 108 mJ/m²。然后研究 He 原子在晶格中不同位置的形成能(E_f), 发现 He 原子在镍金属晶体的张力区域受到晶格的吸引, 而其在压缩区域则受到晶格排斥。通过探讨 He 原子与刃型位错之间的相互作用发现, 相比于置换 He 原子而言, 间隙 He 原子对位错迁移行为的影响更强烈。最后, 研究表明间隙 He 原子的迁移在第一个分位错跨过后表现更明显, 同时刃型位错也为 He 原子迁移提供了更快速的扩散路径。

关键词: 运动行为; 刃型位错; 氦; 原子模拟; 镍

(Edited by Mu-lan QIN)